

DESTABILIZATION OF A SOLAR PROMINENCE/FILAMENT FIELD SYSTEM BY A SERIES OF EIGHT HOMOLOGOUS ERUPTIVE FLARES

NAVDEEP K. PANESAR¹, ALPHONSE C. STERLING², DAVINA E. INNES³, RONALD L. MOORE^{1,2}

¹Center for Space Plasma and Aeronomic Research (CSPAR), UAH, Huntsville, AL 35805, USA

²Heliophysics and Planetary Science Office, ZP13, Marshall Space Flight Center, Huntsville, AL 35812, USA and

³Max Planck Institut für Sonnensystemforschung, Justus-von-Liebig-Weg 3, 37077 Göttingen, Germany

Draft version March 5, 2022

ABSTRACT

Homologous flares are flares that occur repetitively in the same active region, with similar structure and morphology. A series of at least eight homologous flares occurred in active region NOAA 11237 over 16 - 17 June 2011. A nearby prominence/filament was rooted in the active region, and situated near the bottom of a coronal cavity. The active region was on the southeast solar limb as seen from SDO/AIA, and on the disk as viewed from STEREO/EUVI-B. The dual perspective allows us to study in detail behavior of the prominence/filament material entrained in the magnetic field of the repeatedly-erupting system. Each of the eruptions was mainly confined, but expelled hot material into the prominence/filament cavity system (PFCS). The field carrying and containing the ejected hot material interacted with the PFCS and caused it to inflate, resulting in a step-wise rise of the PFCS approximately in step with the homologous eruptions. The eighth eruption triggered the PFCS to move outward slowly, accompanied by a weak coronal dimming. As this slow PFCS eruption was underway, a final 'ejective' flare occurred in the core of the active region, resulting in strong dimming in the EUVI-B images and expulsion of a coronal mass ejection (CME). A plausible scenario is that the repeated homologous flares could have gradually destabilized the PFCS, and its subsequent eruption removed field above the active region and in turn led to the ejective flare, strong dimming, and CME.

Subject headings: Sun: prominences, filaments — Sun: flares — Sun: coronal mass ejections (CMEs)

1. INTRODUCTION

Prominence eruptions are spectacular solar events. They frequently occur in conjunction with solar flares and coronal mass ejections (CMEs) (Munro et al. 1979; Moore 1988; Low 1996). Thus, erupting prominences can be viewed as indirect indicators of likely-impending CMEs. Observational studies of filament motions can tell us about the evolution of coronal magnetic field during solar eruptions (Shibata et al. 1995; Moore et al. 2001; Sterling et al. 2012). It is important to study prominence eruptions for better understanding of erupting coronal magnetic structures.

Prominences are located along the magnetic neutral line in the highly sheared core field of enhanced magnetic regions (Mackay et al. 2010; Labrosse et al. 2010) and prominence plasma is plausibly embedded in a canopy of overlying magnetic field lines, also known as coronal arcades. Except in the immediate vicinity of the neutral line, the enveloping coronal arcade is nearly potential (nearly orthogonal to the neutral line) and confines the prominence plasma and coronal cavity (Low 1994; Hudson & Schwenn 2000). A coronal cavity is the feature sometimes visible on the limb as a dark, low-density region between the prominence and the coronal arcade (Gibson & Fan 2006; Gibson et al. 2010). The coronal cavity is most visible when the prominence and coronal arcade are viewed end-on. Sometimes the cavity is observed on top of the cool prominence material (Régnier et al. 2011; Panesar et al. 2014) and sometimes surrounding the prominence (Berger et al. 2012; Panesar et al. 2013; Schmit & Gibson 2013).

Highly sheared magnetic field plays an important role in the equilibrium of prominences. Processes such as magnetic re-

connection cause the low-lying sheared field to erupt, carrying the prominence material with it (van Ballegoijen & Martens 1989; van Ballegoijen & Cranmer 2010). A prominence is in equilibrium when the downward magnetic tension force balances the upward magnetic pressure force (Priest et al. 1989; Low & Hundhausen 1995). If this force balance becomes disrupted, the field may lose its equilibrium and give rise to the initiation of an eruption. However, it is not necessary that all of the prominence material escapes the Sun. Observational studies show a wide range of prominence eruptions, e.g., ejective and confined eruptions (Ji et al. 2003; Sterling et al. 2012; Kuridze et al. 2013); see also Török & Kliem (2005) for MHD simulations of coronal flux ropes. In the case of confined eruptions a filament is seen to rise and abortively erupt without a CME, whereas in ejective eruptions a filament fully erupts along with a CME (Gilbert et al. 2001; Moore et al. 2001; Török & Kliem 2005). It has been reported by Munro et al. (1979) that 70% of CMEs involve prominence eruptions or disappearances. A large number of theoretical models have been proposed to explain the initiation of solar eruptions, e.g., tether cutting (Moore et al. 2001), magnetic breakout (Antiochos et al. 1999) and flux emergence (Chen & Shibata 2000), etc. Based on observations, it has been suggested that ejective eruptions produce long-duration flares in comparison to confined eruptions (Wang et al. 2007; Cheng et al. 2011).

Coronal dimmings are indirect signatures of CME expulsions in coronal images. It has been reported that dimmings can begin ~ 30 minutes before the appearance of CMEs (Stewart et al. 1974a,b; Rust 1976; Harrison & Lyons 2000). In some cases they begin ~ 3 hours before the CME onset (e.g. Gopalswamy et al. 2001). In addition to accompanying CMEs, they also accompany filament and prominence

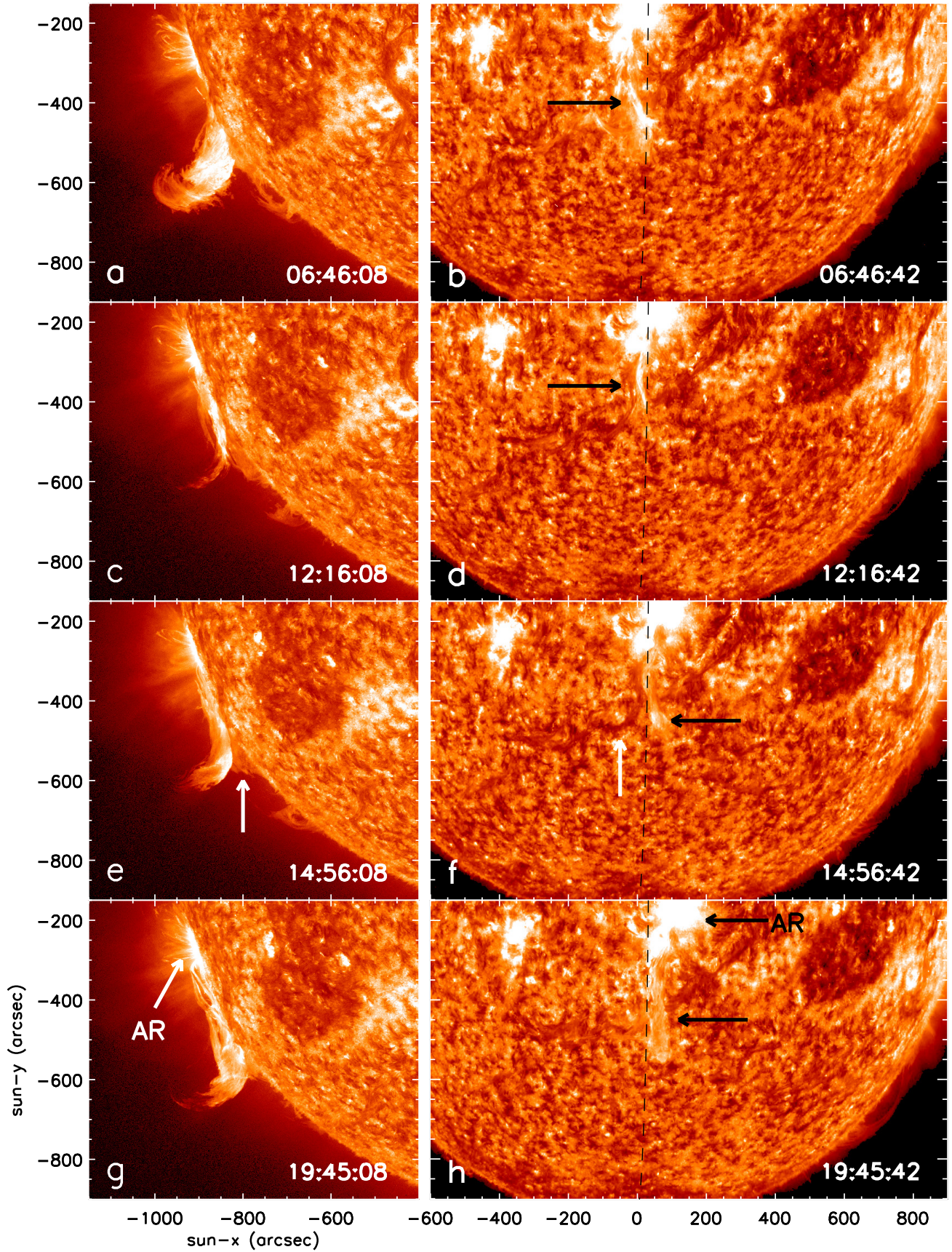


FIG. 1.— Homologous flares observed on 16 June 2011: (left) AIA 304 Å intensity images; (right) corresponding EUVI-B 304 Å intensity images. On the EUVI images, the black dashed line shows the position of the AIA limb in the images on the left. In (e) and (f), the white arrows point to the prominence/filament cavity system (PFCS). In (b), (d), (f) and (h), the black arrows show hot material ejected from the core of the active region during the flares. The Y-axis is the same for all images in both columns. North is upward and west is to the right in these images, and in all other solar images in this paper.

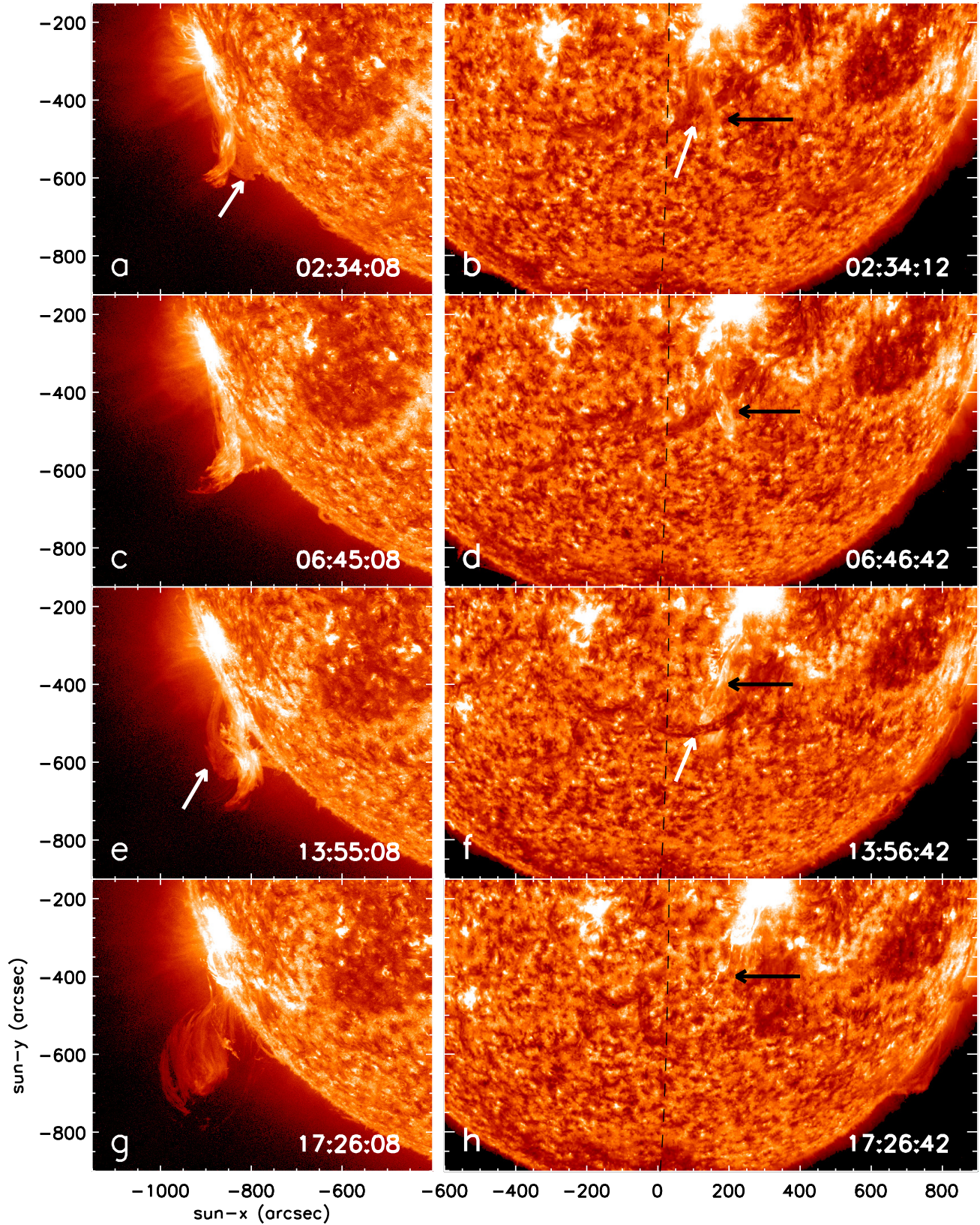


FIG. 2.— Homologous flares observed on 17 June 2011: (left) AIA 304 Å intensity images; (right) corresponding EUVI-B 304 Å images. In (e) and (f), the white arrows point to the erupting prominence/filament. Annotated features are same as those in Figure 1.

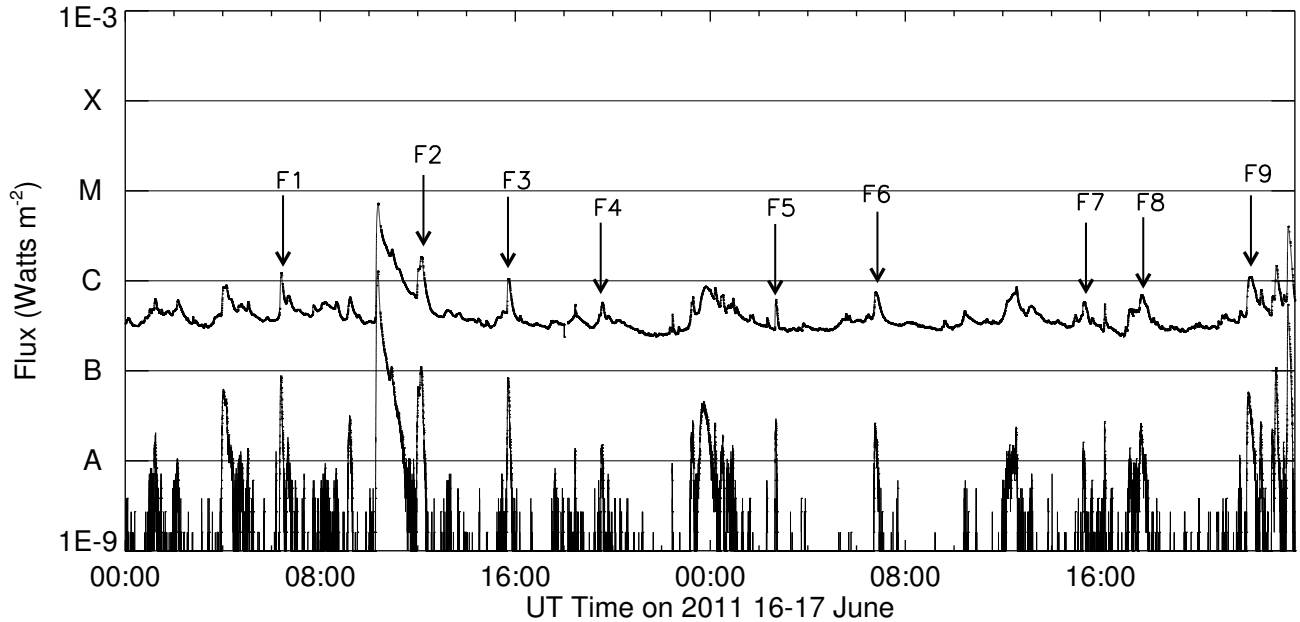


Fig. 3.— *GOES* soft X-ray flux in 1.0 - 8.0 Å and 0.5 - 4.0 Å passbands from 16 to 17 June 2011 showing the nine flares discussed in this paper from active region NOAA 11237. The arrows are drawn at the flare (F1 to F9) times.

eruptions (Gopalswamy & Hanaoka 1998; Harrison & Lyons 2000; Kiepenheuer 1964; Harrison 2003). Basically, coronal dimming is a drop in emission due to the removal/transport of coronal plasma during eruptions. It has been observed that the dimmings can cover either small or large areas of the Sun (Zhukov & Veselovsky 2007; Innes et al. 2010).

Prominence eruptions have rarely been discussed in the context of homologous flares (Chandra et al. 2011; Bocchialini et al. 2012). These are flares that occur repetitively from the same active region, with similar shape, morphology, and footpoints (Waldmeier 1938; Woodgate et al. 1984) as seen in $H\alpha$, EUV and in soft X-ray emission (Martres et al. 1984; Martres 1989; Ranns et al. 2000; Sterling & Moore 2001; Chandra et al. 2011). It is an important phenomena to study because it sheds light on the conditions of the flare trigger processes and on the mechanisms of energy storage and release. These types of series of events suggest that either there is a continuous amount of magnetic energy supplied to an active region, or that not all of the available free energy is released during the eruptions (Schrijver 2009). During homologous flares continuous flux emergence in the flaring active region has been reported by Ranns et al. (2000), Sterling & Moore (2001) and Nitta & Hudson (2001).

In the present work, we report on observations of eight homologous eruptive flares that took place adjacent to a prominence. We mainly focus on the dynamics of the prominence/filament cavity system driven by the flare eruptions using the observations recorded by the Atmospheric Imaging Assembly (AIA) onboard the Solar Dynamics Observatory (SDO), and the Extreme UltraViolet Imager (EUVI) onboard the Solar TERrestrial RELations Observatory (STEREO). We will show that each of the eight flares was a confined eruption, with each eruption expelling field into the prominence/filament field system. The expelled field interacted with the prominence/filament cavity system, and each of the homologous eruptions thereby successively relaxed the stress holding down that prominence/filament cavity. Consequently,

the prominence/filament cavity rose in height in successive steps, until it became destabilized and erupted after the final homologous event. This eruption of the prominence/filament cavity system apparently removed overlying field from the homologous-flare-producing active region, so that the next eruption from that active region was not confined. We infer that the prominence/filament cavity eruption in combination with the final eruption from the active region resulted in a CME that we observed in SOHO/LASCO. To the best of our knowledge, prominence eruptions triggered by homologous flares have never been reported before.

2. INSTRUMENTATION AND DATA

The eight homologous flares were observed by SDO/AIA (Lemen et al. 2012) on the southeast solar limb. Each flare was concurrently observed as an on-disk event occurring near the central meridian in STEREO/EUVI-B (Howard et al. 2008) images. They occurred in active region NOAA 11237 over 16 - 18 June 2011. We study the dynamics of a prominence/filament cavity system that was magnetically connected to the flare eruptions by combining the observations from the two directions. During this period (16-18 June 2011), Hinode was observing elsewhere, and therefore has no data for these events.

Our main data for the limb view are EUV images from SDO/AIA. AIA provides full-Sun images with a high spatial resolution ($0.6'' \text{ pixel}^{-1}$) and high temporal cadence ($\sim 12\text{s}$) in seven EUV wavelength bands (Lemen et al. 2012). We used the images from three channels: 304 Å, which is centered around an He II line (0.05 MK); 171 Å, which is dominated by an Fe IX line (0.7 MK); and 193 Å, which is centered at an Fe XII line formed around 1.5 MK, but also has some response to 0.25 MK plasmas (Del Zanna et al. 2011). For the analysis we mainly used 1- and 5-minute cadence image sequences. We removed the average coronal background from 171 and 193 Å images to enhance the visibility of the coronal

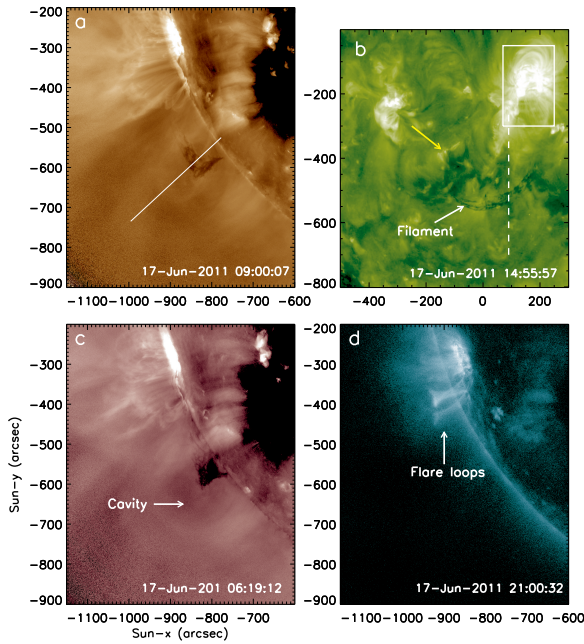


FIG. 4.— Prominence/Filament cavity system: a), c) and d) show AIA 193, 211 and 94 Å intensity images, respectively; b) shows EUVI-B an 195 Å intensity image. In (a), the white diagonal line shows the position of the time-series in Figure 5a. In (b), the white dashed line shows the position of the time-series in Figure 5b and 9. The yellow arrow in (b) indicates the brightening at the remote footpoint of the filament during F7. The boxed region in (b) shows the location of the light curve in Figure 5c.

cavity and overlying coronal structures. The background image was computed by taking the mean of three months of data over May - July 2011. We also examined in a cursory fashion images from the 211 Å and 94 Å channels, formed around 1.9 MK and 6.0 MK, respectively.

Magnetograms from the Helioseismic and Magnetic Imager (HMI) aboard SDO are also used to examine the photospheric magnetic field. HMI provides full-disk line-of-sight magnetograms with high spatial resolution of $0.5'' \text{ pixel}^{-1}$ and temporal cadence of $\sim 45\text{s}$ (Scherrer et al. 2012). A few HMI magnetograms have been used to examine the line-of-sight photospheric magnetic field of the region of interest on 19 June 2011, when the active region was clearly visible on the disk.

For the disk perspective, we used 195 Å and 304 Å EUVI-B images with a spatial resolution of $1.6'' \text{ pixel}^{-1}$ and temporal cadence of $\sim 5\text{-minutes}$ and $\sim 10\text{-minutes}$, respectively. The STEREO 195 Å and 304 Å images are centered around the same Fe XII (1.5 MK) and He II (0.05 MK) lines as the AIA 193 Å and 304 Å images. To identify mutual features in the EUVI-B on-disk-perspective images and in the AIA limb-perspective images, we first selected sub-images of about the same-sized field of view from both instruments, centered on approximately the same feature as seen from the two perspectives. Since EUVI-B has much coarser cadence than AIA, we then selected out AIA images that were from about the same time as the corresponding EUVI-B images. With these images we constructed movies (of $\sim 5\text{ min}$ cadence) from the two instruments. Viewing the so-processed pair of movies (especially but not exclusively in corresponding wavelengths,

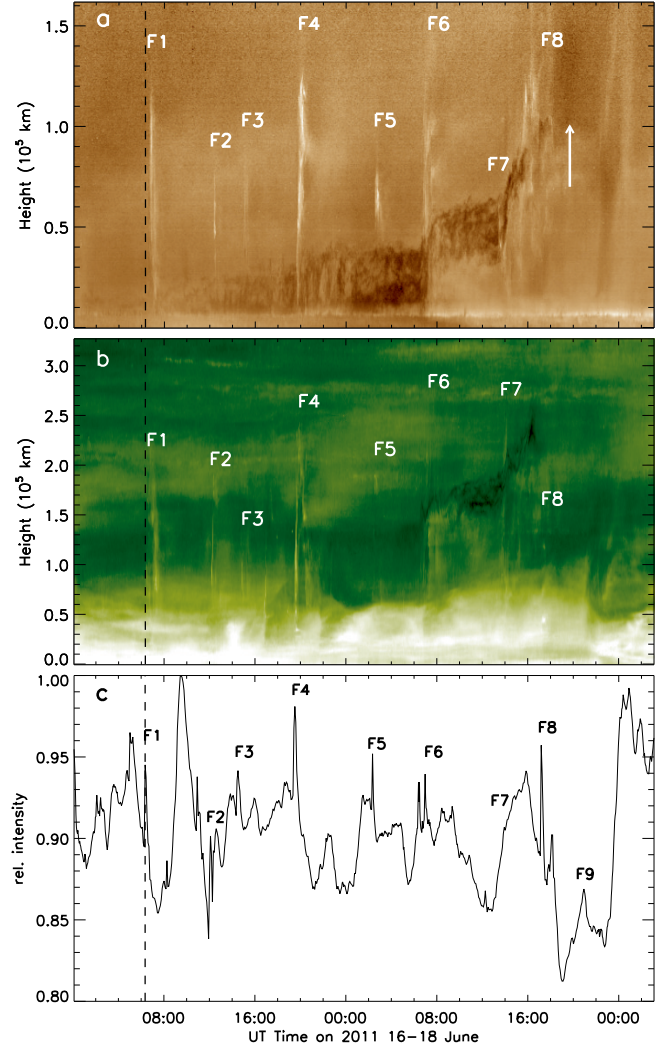


FIG. 5.— Prominence/Filament trajectories: a) AIA 193 Å intensity time-series image along the diagonal line in Figure 4a; b) EUVI-B 195 Å intensity time-series image along the dashed line in Figure 4b; c) EUVI-B 195 Å integrated intensity plot of the region selected in the box shown in Figure 4b. Nine flares are labeled as F1-F9. In (a), the arrow points to the weak dimming after F8.

meaning 304 Å images for AIA and EUVI-B, and 193 Å and 195 Å respectively for AIA and EUVI-B) greatly facilitated identification of the mutual features. The STEREO images have been derotated to a particular time. To show the exact position of the AIA limb features on the EUVI-B 304 Å disk images, we plotted the SDO limb line on the STEREO images (Figure 1 and Figure 2). We also created EUVI-B base-difference images to show better changes in faint structures. We created movies from the various sets of images, to study the events in detail.

3. OBSERVATIONS

3.1. The eight homologous flares

In Figures 1 and 2, we show AIA 304 Å and EUVI-B 304 Å images of the eight homologous flares from active region NOAA 11237 on 16 and 17 June 2011. Over that period, NOAA 11237 was a matured active region on the eastern limb of the Sun. Figure 3 shows the *GOES*-15 soft X-ray

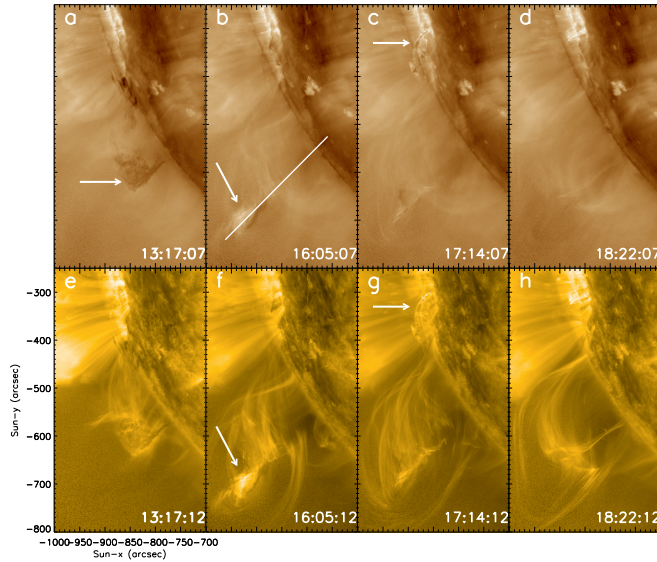


FIG. 6.— Evolution of prominence on 17 June 2011: (a-d) AIA 193 Å intensity images; (e-h) AIA 171 Å intensity images. The arrow points to the prominence in (a). In (b) and (f), the arrows point to the brightening at the top of the prominence. The diagonal line in (b) marks the position of the time-series shown in Figure 7a,b. The arrows in (c) and (g), indicate the brightening in the core of the active region during F8.

flux time profile from 16 to 17 June 2011. From this we can obtain information about the X-ray classes of the flares and the peak-intensity times. We identified nine peaks, during nine flares from NOAA 11237, which we identified from the movies (MOVIE304 and MOVIE193) and flare lists^{1, 2}. The nine flares are highlighted with the arrows from F1 to F9. The first eight of these (F1-F8) correspond to the eight homologous flares shown in Figures 1 and 2, and the ninth (F9) corresponds to the ejective flare from the region. Four of these flares were on 16 June 2011: the first three were C-class and the last one was of B-class. The remaining five were on 17 June 2011: the first four were B-class and the fifth was C-class. Besides F1-F9, a few other small peaks in the GOES plot (including the C flare just before F2) were from the same active region, but appear to be independent of the features we are focusing on here; some of those brightenings are discussed near the end of Section 3.1 Apart from the studied active region, three more active regions were visible during these days. Some other significant peaks in the GOES plot are due to activity from the other three active regions.

We observed a prominence/filament cavity system (PFCS) adjacent to the active region, shown with white arrows in Figure 2a,b. The cavity was discernible only for a few hours on 17 June 2011, surrounding the prominence. It is apparent in the 193 Å and 211 Å images (Figure 4a,c). When referring to the cool material of the PFCS in this paper, we use the term ‘prominence’ for the limb view, ‘filament’ for the disk view, and ‘prominence/filament’ for both limb/disk views. The core of the active region was separated by $\sim 200''$ from the prominence’s spine. From STEREO images, we can see that the prominence is behind the limb from the SDO perspective on 16 June 2011 (Figure 1b). One of the footpoints of the prominence/filament is anchored in the active region (Figure 1d) and the other footpoint is southeast of the active region in a quiet-Sun location, as we can see in the STEREO images

¹ http://hesperia.gsfc.nasa.gov/hessidata/dbase/hessi_flare_list.txt

² http://www.lmsal.com/solarsoft/latest_events_archive.html

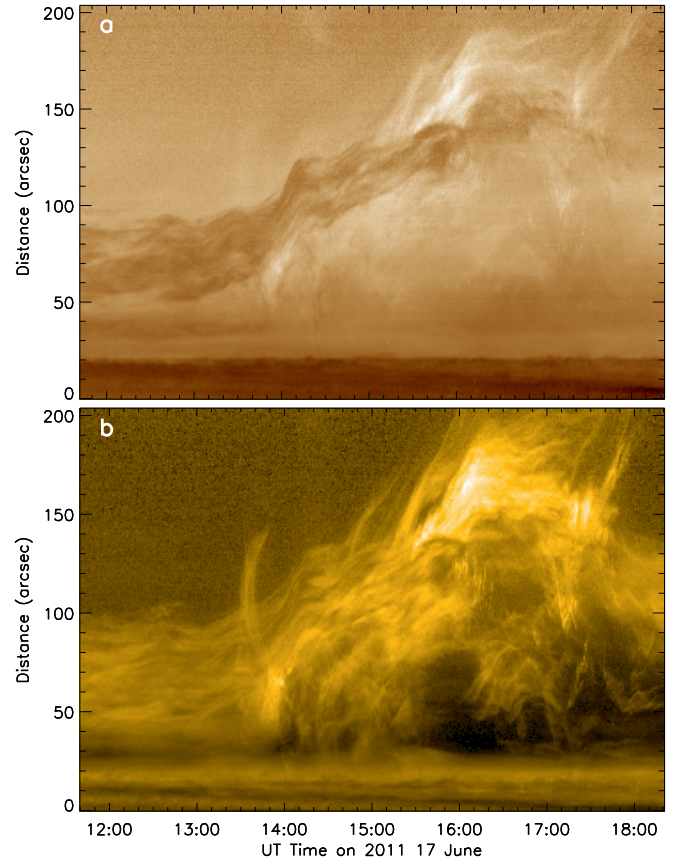


FIG. 7.— Prominence eruption on 17 June 2011: (a) AIA 193 Å and (b) 171 Å intensity time-series image along the diagonal line in Figure 6b. Initially, the prominence rises at 13:50 UT, and then it starts to fall toward the solar surface at 17:05 UT.

(Figure 2b). The active region and prominence/filament is the part of the same system. To relate the line-of-sight magnetograms with on-disk structures in the EUVI-B images, we looked at HMI images taken two days later, on 19 June 2011, when the active region and magnetic neutral line were more clearly visible on the SDO disk images. For this purpose, we summed 30-minutes worth of 45-second cadence co-aligned HMI magnetograms, thereby building a single deep magnetogram. The filament and its far footpoint (i.e the footpoint farthest from the active region, shown in Figure 4b) resided in a weak-field region, based on the SDO/HMI line-of-sight magnetogram of the region on 19 June 2011 (Figure 10).

Here we discuss in more detail the nine flares from the active region and the material ejected along with these flares, as seen from AIA and EUVI-B. Figure 1 and 2 show the concurrent brightenings in both images during the flares (shown with black arrows on STEREO images). The repeated flares from the same active region, from the same position, certainly come under the category of homologous flares, discussed by, e.g. Woodgate et al. (1984) and Choe & Cheng (2000). A close-up view of the homologous flares is shown in Figure 11a,b and in MOVIEAIA. All of the eight homologous flares were accompanied by confined eruptions. Each of the homologous flares had the same pattern, with a brightening at the flaring location, followed by ejection of material (shown with black arrows in Figure 1b and 2b) and field from the flaring region. That ejecta interacted with the PFCS, and successively disrupted the overall stability of that system. In Figures 2e and 2f, the white arrows point to the activated

prominence/filament after flare F8. The flares' onsets and related prominence/filament response can be seen in the 304Å movie accompanying Figure 1 and 2.

A note on our use of “confined”- and “ejective”-eruption terminology: In this paper we say that the eight homologous flares, F1-F8, are “confined,” even though each of these eruptions expelled ejecta. More specifically, our meaning is that each of these eight flares ejected material only out of their immediate vicinity, i.e. the ejecta left the active region in which those flares occurred. But, in each of these eight cases, the so-ejected material became trapped within the field of the PFCS, and therefore that material did not leave the Sun and form a CME, as in canonical ejective flares. In this sense, the eight homologous flares were not completely confined or completely ejective, as used in standard solar terminology. Our convention here is to say that they were confined, because their ejected material did not escape from the Sun as a CME. This is in contrast to the case of flare F9, which was clearly ejective because its expelled material left the Sun, as we will discuss later.

To explain the general progression of the homologous eruptions, in this paragraph we discuss the progression of events around the time of homologous flare F6; we refer the reader to MOVIE193 accompanying this paper. The flare started at 06:20 UT on 17 June 2011. There was a brightening in the south of the active region (at the magnetic neutral line, Figure 10) at 06:20 UT, see MOVIE193. At 06:25 UT some hot material, together with magnetic field, was ejected from the core of the active region as typically happens according to the standard model for solar eruptions (e.g. Shibata et al. 1995; Moore et al. 2001). At the same time the ejection of the hot material is also seen in the EUVI-B 195 Å images as bright ejecta. This bright ejecta hit the prominence/filament at 06:45 UT and resulted in an upward rise of the prominence/filament. The ejecta became trapped in the cavity field lines, which were connected to the PFCS. The AIA limb images clearly show the movement of bright material along the cavity field lines at 06:50 UT. Simultaneously, we can see that the brightening swept over the filament and the remote footpoint of the filament brightened (indicated by an arrow in Figure 4b during F7). The brightening is faintly visible in the EUVI-B frames of MOVIE193 at 07:25 UT, which is after F6. All eight homologous events followed this same basic pattern with only slight variations. In particular, after F8, the prominence/filament disappeared and the cool material drained to the solar surface. The field containing the PFCS continued to expand slowly after F8 and completely removed overlying field from above the active region.

The last flare, F9, occurred at $\sim 21:00$ UT. It was an ejective eruption (flare loops are shown in Figure 4d). A CME followed the last flare, F9. The CME is detected by LASCO as shown in Figure 8c. According to the LASCO catalog³, the CME material had a velocity of ~ 234 km s⁻¹. If we follow the linear fit of the plane-of-sky velocity back in time, it matches well with the flare (F9) timing. This suggests that the CME occurred in conjunction with F9.

To see the relation between prominence/filament motion and the flares, we construct height-time plots over two cuts: one along the prominence in AIA images (Figure 4a), and the other across the filament in EUVI-B images (Figure 4b). Figure 5a,b shows the height of the filament as a function of

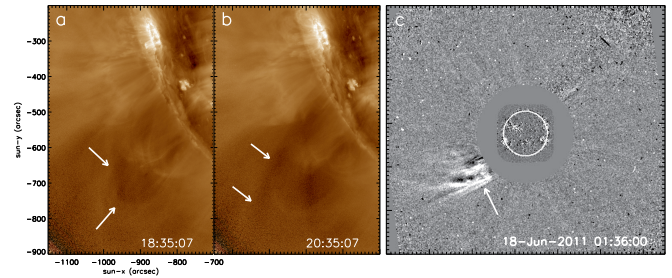


FIG. 8.— Coronal arcade and CME: (a-b) AIA 193 Å intensity images. The white arrows point to the expansion of the overlying coronal field after F8. (c) LASCO (C2) and AIA 193Å running-difference image; an arrow indicates the CME after F9.

time, along the fiducial lines plotted in Figure 4a,b. In the time-series image, the eight homologous flares are marked as F1 to F8. The filament trajectory is not visible before F6 in Figure 5b, because the position of the fiducial line is close to the active region, away from the center of the filament. We selected the location for the EUVI-B fiducial in Figure 4b so that the bright ejecta from the flares in the active region would cross that fiducial; these bright ejecta are labeled as F1-F8 in Figure 5a. In other words, it is the bright ejecta from the flares crossing the fiducial line that appear as F1-F8 in Figure 5a,b, but the filament itself does not cross the fiducial line (Figure 4b) as it moves prior to F6. Those early-time prominence motions are however well captured in the AIA height-time plot (Figure 5a), which are based on the fiducial line in Figure 4a.

In Figure 5a,b, we show the flare brightenings (vertical bright lines labeled F1-F8) during the eight homologous eruptions, interacting with the prominence/filament. Figure 5a,b shows the relation between the flares and prominence/filament. There is a slow rising motion of the prominence/filament apparent in both SDO and STEREO time-series images (Figure 5a,b). There are conspicuous jumps in the prominence trajectory after F4, F6 and F7. The prominence does not show any increase in height during F3 and F5 (Figure 5a). Before F3, the prominence was beyond the SDO limb, therefore it is not clearly visible in SDO time-series image (in Figure 5a). Figure 5a covers three important dynamics of the prominence: (1) the prominence enters its fast-rise phase at 13:50 UT on 17 June 2011, (2) the prominence disappears completely with F8, and (3) a coronal dimming (indicated with an arrow in Figure 5a) starts after the eruption F8.

In Figure 5c, we show a light curve of a sub-region of the EUVI-B images from 16 to 17 June 2011. This is an integrated intensity plot of the region inside the box shown in Figure 4b. The intensity profile shows the apparent increase in intensity during each of the nine flares, F1-F9. The AIA and EUVI-B intensity time-series images show the flare brightenings occurring just after the flares (e.g. dashed line during F1 in Figure 5a,b) because the fiducial lines are not centered in the core of the active region. The EUVI-B 195Å light curve also shows several other intensity peaks; these are due to the sudden increase in brightening in the north of the active region loops. Figure 5c shows multiple peaks during F7. We checked this carefully and observed that there are two more apparent brightenings in the active region (at $\sim 14:00$ and $15:50$ UT) between F7 and F8. These brightenings are prominent in the AIA 94Å images. It seems as if there was a cascade of loop brightenings between 13:00 and 16:00 UT, explaining

³ http://cdaw.gsfc.nasa.gov/CME_list

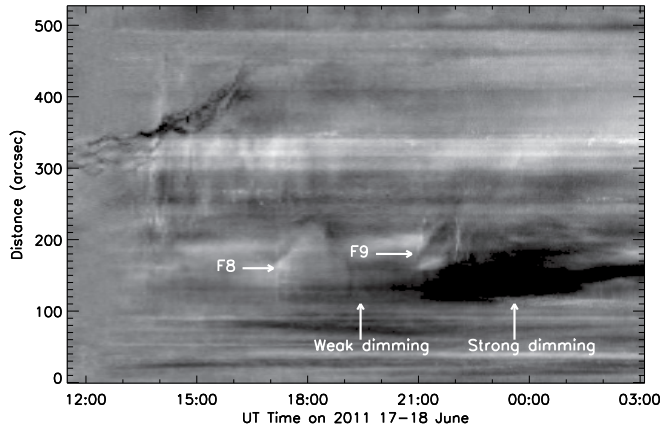


FIG. 9.— Coronal dimming: EUVI-B 195 Å base-difference time-series image along the dashed line in Figure 4b. The weak and strong coronal dimming is apparent after F8 and F9, respectively. The subtracted base image time was obtained by averaging images between 11:45 and 13:00 UT.

the multiple peaks during F7 in Figure 5c. We also find that there is an intensity drop around F9 (in Figure 5c), which is due to the dimming before and after F9 (see Figure 9). We can also compare the integrated intensity plot of Figure 5c with the soft X-ray flux measured by *GOES* in Figure 3. The light curve for the EUVI-B 195Å channel shows peak times of the nine flares to be at the same times as the *GOES* peak times.

3.2. Prominence eruption

Examining the motion of the prominence, we find that there is a slow-rise after F4, near 20:00 UT (Figure 5a), followed by a relatively flat plateau (before F6) in the prominence slow-rise phase. After the sixth flare, F6, which was at $\sim 07:26$ UT, the prominence/filament starts to rise again (see Figure 5a,b). This slow motion continues for the next ~ 6 hours. There is an unambiguous rise in the prominence/filament height after F7, at 13:50 UT. With F7, the prominence/filament becomes destabilized and begins to rise further at a relatively faster speed; we say that the prominence/filament enters its fast-rise phase at this time. It subsequently reaches to a maximum height, before the prominence/filament plasma drains down towards the solar surface. The fast-rise of the filament lasts for 3 hours, between $\sim 13:50$ and 17:05 UT. Finally, it detaches from the solar surface with the last homologous flare, F8, which peaked at 17:08 UT (according to the RHESSI⁴ flare list). We also measured the velocities of the prominence rise during its slow-rise and fast-rise by following the motion of the prominence along the fiducial line (in Figure 4a). The prominence moves with an average velocity of $\sim 1 \text{ km s}^{-1}$ between 07:30 UT and 14:00 UT during its slow-rise phase. During the fast-rise phase (after F7), it moves with an average velocity of $\sim 4 \text{ km s}^{-1}$.

To see the evolution of the prominence during its eruption, we create a distance-time image along the white diagonal line in Figure 6b. Figure 7a,b shows the upward motion of the prominence, which starts at $\sim 13:50$ UT. A brightening appears near the top of the prominence at $\sim 15:30$ UT (see MOVIE193). Strong downflows appear in 171Å and 193Å after the brightening at the top (see Figure 7). We suspect that the brightening was due to magnetic reconnection between the field containing the flare ejecta, and the field carrying the fil-

ament material during F7. This brightening is clearly visible in AIA 304, 171, 193 and 211 Å channels, but not in the 94 Å channel. This suggests that these brightenings were low-level ($\sim 2 \text{ MK}$) heating events. Finally, the prominence material falls back towards the solar surface. Possibly, the field containing the PFCS did not allow the prominence material to escape. At least at this time, there was no complete opening of the field lines.

3.3. Coronal dimming and the CME

Figure 8a,b shows the expansion of the overlying coronal field above the prominence/filament system. The biggest change in that overlying coronal field occurred after F8; F8 erupted at 17:14 UT on 17 June 2011. The overlying field lines started to expand slowly at 17:50 UT (see MOVIE193). They opened completely at about the time of the last flare, F9, at $\sim 21:00$ UT (see Figure 4d). At the same time, we notice a strong dimming to the south of the active region in the EUVI-B 195Å images.

To see the evolution of the dimming with time, we have created a base-difference time-series image (see Figure 9) along the vertical dashed line shown in Figure 4b. For the base image, we averaged ~ 1.5 hours of data prior to F7. The dimming can be clearly seen in the base-difference image. Figure 9 shows both weak and strong dimmings. We notice an appearance of weak dimming just after F8, which is due to expansion of coronal field lines after the filament eruption. Simultaneously, this dimming was observed in the AIA 193 Å images (shown with an arrow in Figure 5a). The strong dimming appears around 21:05 UT (in Figure 9). It occurred after F9, and is clearly a consequence of that F9 eruption.

From the SOHO/LASCO C2 coronagraph, a CME was observed at 00:23 UT on 18 June 2011 (Figure 8c). We expect that the CME originated from the strongly-dimmed region. It is known that dimmings often occur in conjunction with flares and filament eruptions (e.g. Sterling & Hudson 1997; Harra & Sterling 2001; Howard & Harrison 2004), and dimmings are mainly due to density depletion along the line-of-sight (Webb & Howard 2012). From our observations, it appears that the strong dimming results from the removal of coronal material with the last eruption, F9.

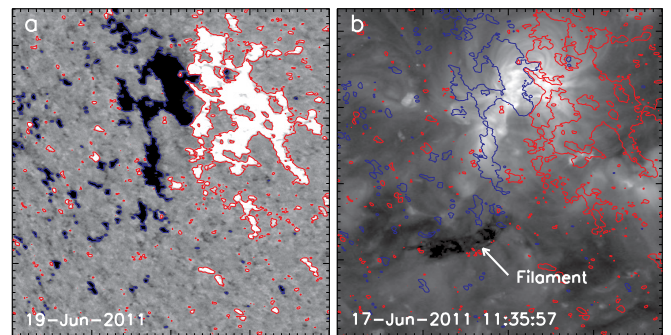


FIG. 10.— a) HMI magnetogram of the active region observed on 19 June 2011; b) EUVI-B 195 Å image of the active region and filament on 17 June 2011, overlaid with the contours of the HMI magnetogram shown in (a). In (a) and (b), the blue and red contours (of $\pm 40 \text{ G}$) represent negative and positive magnetic flux, respectively.

4. DISCUSSION AND SUMMARY

Eight homologous eruptive flares were observed by SDO/AIA and STEREO/EUVI-B in active region NOAA

⁴ http://hesperia.gsfc.nasa.gov/hessidata/dbase/hessi_flare_list.txt

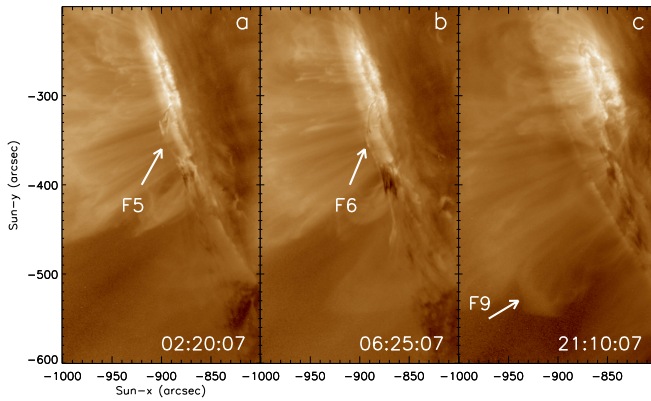


FIG. 11.— Flares on 17 June 2011: (a-c) AIA 193 Å intensity images. In (a), (b) and (c), the arrows point to the F5, F6, and F9, respectively.

11237 over 16 - 17 June 2011. We observed a prominence/filament cavity system (PFCS) that was magnetically connected to the flaring region. The PFCS was continuously disrupted by ejecta expelled into it by the eight homologous eruptions from the nearby active region. We mainly diagnose the 3D dynamics of the PFCS during the series of homologous flares. Over the two-day time period investigated, we found that with each of the first eight homologous flares (F1-F8), some hot material, presumably together with magnetic field, was ejected from the core of the active region. This material and field entered and interacted with the PFCS; this is clearly seen in Figure 1 and 2. This caused the PFCS to rise upwards slowly but significantly in several steps (after F4, F6 and F7).

During the first three flares (F1-F3) on 16 June 2011, the prominence is not fully discernible in the AIA images. Apparently it was beyond the limb, and we confirmed this by looking at in the STEREO images of the filament on the disk (Figure 1b,d,f and MOVIE304). At later times, the prominence response to the flares is clearly discernible in the AIA limb images. By following the motion of the prominence in the AIA 193Å images, we find conspicuous jumps in the prominence trajectory after F4, F6 and F7. A slow-rise motion in the prominence trajectory is observed for ~ 4 -5 hours after F4 ($\sim 20:00$ UT), followed by a plateau in velocity for ~ 4.5 hours after F5. After F6, there is a continuous slow-rise in the prominence/filament trajectory for about 6-7 hours followed by a fast-rise (after F7), for 3 hours, as observed in the SDO and STEREO images. Similar behavior of filament transition from slow-rise to fast-rise has also been studied by e.g., Sterling & Moore (2005) and Sterling et al. (2012). In the present study, the slow-rise and fast-rise are apparently triggered by the flare eruptions from the active region.

Bright ejecta are expelled during each homologous eruption and move along the cavity field lines, and each ejection disturbed the magnetic field holding down the PFCS. Some faint brightenings are observed at the remote filament footpoint (arrow in Figure 4b) in EUVI-B 304 Å and 195 Å images. The prominence/filament begins to rise fast with F7 and it becomes detached completely from the solar surface after F8. Shortly after F8, prominence plasma drains to the solar surface but the overlying field of the PFCS continued to move outward as indicated by the weak dimming in Figures 5a and 9. Basically, each of the eight homologous eruptions gradually weakened the magnetic tension force that maintains the overall stability of the PFCS. The last homologous eruption, F8, removed the enveloping field above the PFCS. Part of that enveloping field also covered the nearby active region, and

removal of that field resulted in the final eruption from that active region, F9, which was ejective.

Figure 11 shows a close-up of the core portion of the active region, which was the site of the origin of flares F1-F9. That figure compares the situation with the confined eruptions, F1-F8, and that of the ejective eruption F9. Figure 11a,b shows the situation that was typical for the confined eruptions: a small-scale ($\sim 50''$) filamentary feature in the core region contained a mixture of absorbing and emitting material. This feature was dynamic, as is apparent from the movies (MOVIE193 and MOVIEAIA), and was located where the principle flare brightenings occurred corresponding to each of the respective confined eruptions. Figure 11a,b shows the behavior of flares F5 and F6, and accompanying MOVIEAIA almost shows that each of the flares F1-F8 display essentially same basic behavior. In contrast, flare F9 showed different behavior in the core region of the active region (see Figure 11c). This morphological difference between F1-F8 on the one hand, and F9 on the other, suggests that either the triggering mechanism for F9 was different from that of the first eight eruptions, or the triggering mechanism was the same but the physical consequences of that mechanism likely were different due to a change in the local magnetic topology resulting from the removal of the overlying field. These physical consequences include the morphological differences illustrated in Figure 11, and another is the production of a CME. During F9, ejected material escaped the Sun as a CME, shown with an arrow in Figure 8c and 11c. In contrast, during the first eight eruptions (F1-F8), the ejected material was trapped in the overlying coronal field, which did not allow the material to leave the Sun (Figure 11a,b). We speculate that the eruption F8 successively removed the overlying field, triggering a final ejective eruption F9, followed by a CME. It is worth mentioning here that last two flares (F8 and F9) might be called sympathetic-like flares because F8 causes the filament to erupt, and then that eruption leads to last flare F9.

Flare F9 follows the catastrophic disruption to the PFCS by flare F8. Unlike the first eight eruptions (F1-F8), F9 was *not* confined. Rather, it apparently was an ejective eruption, resulting in the CME (Figure 8c), and in strong coronal dimming (Figure 9). F9 appears to have originated from approximately the same location in the core of the active region as F1-F8. So why were F1-F8 confined and F9 ejective? We speculate that, when the PFCS was disrupted after F8, the field enveloping the PFCS started to erupt slowly; that is, the field slowly (in 3.5 hours) began to open (see MOVIE193 at 18:55 UT). This slow-field-opening process removed some of the field that had been overlying and confining the F1-F8 flares. With this overlying field removed, the next flare eruption, F9, was able to escape the Sun without being confined. This process is similar to what has been observed by Schrijver & Tittle (2011) and modeled by the Török & Kliem (2005). The process where by overlying field is removed by the first eruption and results in a second eruption was called ‘lid removal’ in Sterling et al. (2014). In the present study, the so-called ‘overlying lid/field’ had been removed by the last homologous eruption, F8, which allowed the F9 eruption to start and to not be confined.

In Figure 12, we summarize our observations with the help of a cartoon. It shows the evolution of the event according to the SDO and STEREO observations. We do not have magnetic field information during our observation period and so the details of this summary are inevitably speculative. Figure 12a represents the situation prior to the final three erup-

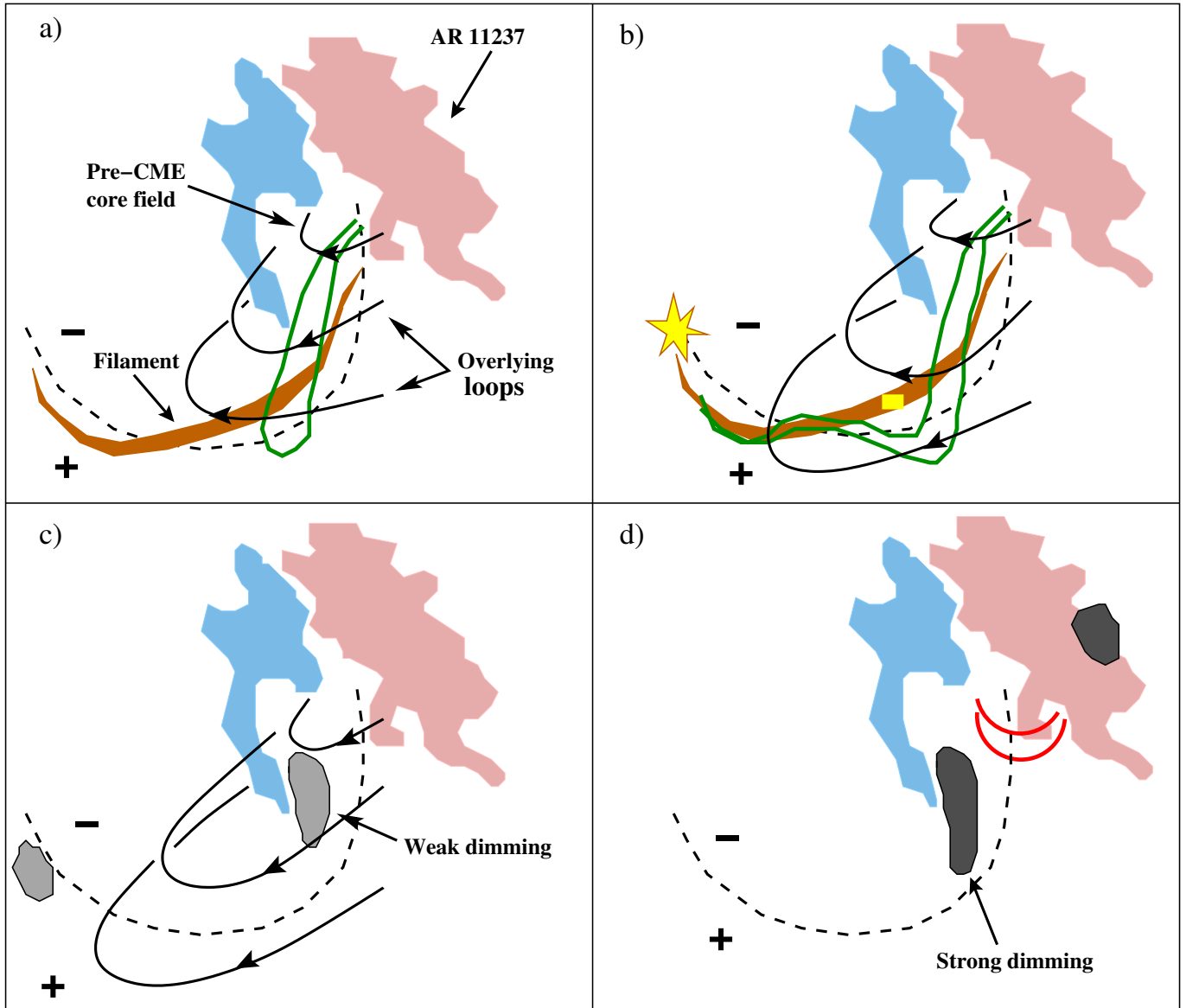


FIG. 12.— Schematic illustration of observations: A STEREO/EUVI-B view of the filament (orange) and active region. Blue and pink patches indicate negative and positive magnetic flux, respectively. The black dashed line roughly outlines the position of the photospheric neutral line. In (a) and (b), the green loop represents material and field ejected from the core of the AR during the eight homologous-flare eruptions, resulting in the reconnection (yellow box in b) with the field holding the filament (the PFCS) and also resulting in an expansion and eventual opening of overlying coronal loops in (b) and (c), followed by a weak coronal dimming in (c). Panel (d) shows the situation following complete removal of overlying loops and the strong coronal dimming after the last eruption, F9; the red arcs indicate the F9 flare loops

tions (F7 to F9). It shows the filament lying along the photospheric neutral line with overlying coronal field lines. A pre-CME core field is shown with an arrow in Figure 12a and Figure 11c. The green line shows the path taken by hot material that ejected from the active region core during the homologous eruptions. Each ejection hit the filament field and destabilized it. More precisely, with each homologous eruption, the flare ejecta, which consisted of hot material and magnetic field in which that material was entrained, struck in a broadside fashion the PFCS field that contains the filament. This concept of the ejecta consisting of hot material and magnetic field is fully consistent with the standard model for solar eruptions. According to the standard model, an eruption expels filament material and field, and both eventually becomes part of a CME (see Figure 1 of Moore et al. (2001) and Figure 1 of Shibata et al. (1995)). In the case of our homologous

eruptions, we are proposing that our ‘ejecta’ correspond to the CME-producing components of this standard-model: the ‘hot material’ of the ejecta corresponds to the expelled filament in the standard model (we are assuming that the filament material underwent some heating during the eruption), and the ‘field’ of the ejecta corresponds to the field surrounding the expelled filament in the standard model. In the standard model as depicted in the above references, the expelled filament and field move out vertically from the Sun. In our homologous flares, the ejecta instead moves out nearly horizontally, and becomes trapped on the larger scale field that wraps around the PFCS.

Figure 12b,c,d shows the filament system after F7, F8, and F9 respectively. The coronal cavity started to expand slowly with the eruption F7, which allowed the filament material to rise further. At the same time, there was a brightening at the

remote filament footpoint (in weak magnetic field), shown by the star in Figure 12b. During each eruption there was an ejection of hot material, as discussed before, which moved along the cavity field and brightened the remote footpoint of the filament (see Figure 12b and accompanying MOVIE193). The filament slowly started moving away from its remote footpoint just after the brightening (after F7 at 14:35 UT) and left a dimming (Figure 12c). In addition to footpoint brightening, one more enhanced brightening is seen at the top of the prominence at 15:30 UT (approximately at the location of the yellow box in Figure 12b; corresponding to the location indicated by the arrow in Figure 6b). The prominence material below the brightening is observed draining towards the surface. Plausibly, the brightening was due to the spatially localized magnetic reconnection between the field containing the flare ejecta, and the field carrying the filament material. This reconnection possibly reconfigured the field lines and led to the observed downflow. The overlying coronal field did not allow the prominence/filament material to escape outward and led to a prominence/filament eruption (Moore et al. 2001). After $\sim 17:50$ UT, the overlying field lines (labeled as ‘overlying loops’ in Figure 12a) visibly expanded over the next 3.5 hours (shown in Figure 12b,c), leading to the weak dimming, and to the last flare, F9, at 21:00 UT (flare loops are shown in Figure 12d, and Figure 4d; they are also visible in

MOVIE193). This suggests that the removal of the field overlying the active region may have triggered the final ‘ejective’ eruption from the core of the active region. Shortly after F9, a region of strong dimming (strong compared to the earlier weaker dimming) occurred close to the negative and positive flux of the active region (Figure 12d). The appearance of the strong dimming over a large surface area just after the flare was presumably due to the expulsion of coronal material with the CME (Harrison & Lyons 2000; Howard & Harrison 2004). The CME was seen at 00:37 UT on 18 June 2011, which was after the strong dimming onset and 3 hours after the start of flare F9. We speculate that the series of homologous eruptions destabilized the PFCS and thereby opened the overlying coronal field, leading to the CME.

We acknowledge the use of the SDO/AIA, STEREO/EUVI observations for this study. SDO data are courtesy of the NASA/SDO AIA and HMI science teams. STEREO data are courtesy of the STEREO Sun Earth Connection Coronal and Heliospheric Investigation (SECCHI) team. This work was supported by the Heliophysics Division of NASA’s Science Mission Directorate through the Living With a Star Targeted Research and Technology Program, and by the Hinode Project.

REFERENCES

- Antiochos, S. K., DeVore, C. R., & Klimchuk, J. A. 1999, *ApJ*, 510, 485
 Berger, T. E., Liu, W., & Low, B. C. 2012, *ApJ*, 758, L37
 Bocchialini, K., Koutchmy, S., Solomon, J., & Tavabi, E. 2012, in *EAS Publications Series*, Vol. 55, *EAS Publications Series*, ed. M. Fauroubert, C. Fang, & T. Corbard, 335–338
 Chandra, R., Schmieder, B., Mandrini, C. H., et al. 2011, *Sol. Phys.*, 269, 83
 Chen, P. F., & Shibata, K. 2000, *ApJ*, 545, 524
 Cheng, X., Zhang, J., Ding, M. D., Guo, Y., & Su, J. T. 2011, *ApJ*, 732, 87
 Choe, G. S., & Cheng, C. Z. 2000, *ApJ*, 541, 449
 Del Zanna, G., O’Dwyer, B., & Mason, H. E. 2011, *A&A*, 535, A46
 Gibson, S. E., & Fan, Y. 2006, *Journal of Geophysical Research (Space Physics)*, 111, 12103
 Gibson, S. E., Kucera, T. A., Rastawicki, D., et al. 2010, *ApJ*, 724, 1133
 Gilbert, H. R., Holzer, T. E., & Burkepile, J. T. 2001, *ApJ*, 549, 1221
 Gopalswamy, N., Cyr, O. C. S., Kaiser, M. L., & Yashiro, S. 2001, *Sol. Phys.*, 203, 149
 Gopalswamy, N., & Hanaoka, Y. 1998, *ApJ*, 498, L179
 Harra, L. K., & Sterling, A. C. 2001, *ApJ*, 561, L215
 Harrison, R. A. 2003, *Advances in Space Research*, 32, 2425
 Harrison, R. A., & Lyons, M. 2000, *A&A*, 358, 1097
 Howard, R. A., Moses, J. D., Vourlidas, A., et al. 2008, *Space Science Reviews*, 136, 67
 Howard, T. A., & Harrison, R. A. 2004, *Sol. Phys.*, 219, 315
 Hudson, H., & Schwenn, R. 2000, *Advances in Space Research*, 25, 1859
 Innes, D., McIntosh, S., & Pietarila, A. 2010, 517
 Ji, H., Wang, H., Schmahel, E. J., Moon, Y.-J., & Jiang, Y. 2003, *ApJ*, 595, L135
 Kiepenheuer, K. O. 1964, *NASA Special Publication*, 50, 323
 Kuridze, D., Mathioudakis, M., Kowalski, A. F., et al. 2013, *A&A*, 552, A55
 Labrosse, N., Heinzel, P., Vial, J.-C., et al. 2010, *Space Sci. Rev.*, 151, 243
 Lemen, J. R., Title, A. M., Akin, D. J., et al. 2012, *Sol. Phys.*, 275, 17
 Low, B. C. 1994, *Physics of Plasmas*, 1, 1684
 —. 1996, *Sol. Phys.*, 167, 217
 Low, B. C., & Hundhausen, J. R. 1995, *ApJ*, 443, 818
 Mackay, D. H., Karpen, J. T., Ballester, J. L., Schmieder, B., & Aulanier, G. 2010, *Space Sci. Rev.*, 151, 333
 Martres, M. J. 1989, *Sol. Phys.*, 119, 357
 Martres, M.-J., Mouradian, Z., & Soru-Escaut, I. 1984, *Advances in Space Research*, 4, 31
 Moore, R. L. 1988, *ApJ*, 324, 1132
 Moore, R. L., Sterling, A. C., Hudson, H. S., & Lemen, J. R. 2001, *ApJ*, 552, 833
 Munro, R. H., Gosling, J. T., Hildner, E., et al. 1979, *Sol. Phys.*, 61, 201
 Nitta, N. V., & Hudson, H. S. 2001, *Geophys. Res. Lett.*, 28, 3801
 Panesar, N. K., Innes, D. E., Schmit, D. J., & Tiwari, S. K. 2014, *Sol. Phys.*, 289, 2971
 Panesar, N. K., Innes, D. E., Tiwari, S. K., & Low, B. C. 2013, *A&A*, 549, A105
 Priest, E. R., Hood, A. W., & Anzer, U. 1989, *ApJ*, 344, 1010
 Ranns, N. D. R., Harra, L. K., Matthews, S. A., & Culhane, J. L. 2000, *A&A*, 360, 1163
 Régnier, S., Walsh, R. W., & Alexander, C. E. 2011, *A&A*, 533, L1
 Rust, D. M. 1976, *Sol. Phys.*, 47, 21
 Scherrer, P. H., Schou, J., Bush, R. I., et al. 2012, *Sol. Phys.*, 275, 207
 Schmit, D. J., & Gibson, S. 2013, *ApJ*, 770, 35
 Schrijver, C. J. 2009, *Advances in Space Research*, 43, 739
 Schrijver, C. J., & Title, A. M. 2011, *Journal of Geophysical Research (Space Physics)*, 116, 4108
 Shibata, K., Masuda, S., Shimojo, M., et al. 1995, *ApJ*, 451, L83
 Sterling, A. C., & Hudson, H. S. 1997, *ApJ*, 491
 Sterling, A. C., & Moore, R. L. 2001, *J. Geophys. Res.*, 106, 25227
 —. 2005, *ApJ*, 630, 1148
 Sterling, A. C., Moore, R. L., Falconer, D. A., & Knox, J. M. 2014, *ApJ*, 788, L20
 Sterling, A. C., Moore, R. L., & Hara, H. 2012, *ApJ*, 761, 69
 Stewart, R. T., Howard, R. A., Hansen, F., Gergely, T., & Kundu, M. 1974a, *Sol. Phys.*, 36, 219
 Stewart, R. T., McCabe, M. K., Koomen, M. J., Hansen, R. T., & Dulk, G. A. 1974b, *Sol. Phys.*, 36, 203
 Török, T., & Kliem, B. 2005, *ApJ*, 630, L97
 van Ballegooijen, A. A., & Cranmer, S. R. 2010, *ApJ*, 711, 164
 van Ballegooijen, A. A., & Martens, P. C. H. 1989, *ApJ*, 343, 971
 Waldmeier, M. 1938, *ZAp*, 16, 276
 Wang, T., Innes, D. E., & Qiu, J. 2007, 656, 598
 Webb, D. F., & Howard, T. A. 2012, *Living Reviews in Solar Physics*, 9, 3
 Woodgate, B. E., Martres, M.-J., Smith, Jr., J. B., et al. 1984, *Advances in Space Research*, 4, 11
 Zhukov, A. N., & Veselovsky, I. S. 2007, *ApJ*, 664, L131